DOI: 10.1021/cg100596q

CRYSTAL GROWTH & DESIGN Article

2010, Vol. 10
3996–4004

Additive-Assisted Aqueous Synthesis of $BaTiO_3$ Nanopowders

Florentina Maxim,[†] Paula Ferreira,[†] Paula M. Vilarinho,*[,†] Anne Aimable,[‡] and Paul Bowen[‡]

[†]*Department of Ceramics and Glass Engineering, Centre for Research in Ceramics and Composite Materials, CICECO, University of Aveiro, 3810-193 Aveiro, Portugal, and* [‡]*Powder Technology Laboratory, Materials Department, Swiss Federal Institute of Technology Lausanne (EPFL), Switzerland*

Received May 4, 2010; Revised Manuscript Received July 20, 2010

ABSTRACT: The effect of poly(acrylic acid) (PAA), poly(vinylpyrrolidone) (PVP), sodium dodecylsulfate (SDS), hydroxypropylmethylcellulose (HPMC), and D-fructose additives on the growth of $BaTiO_3$ particles by aqueous synthesis is studied. Through different mechanisms, all the tested additives influenced the growth of $BaTiO_3$. For high concentrations, PAA adsorbed on specific crystallographic faces changing the growth kinetics and inducing the oriented attachment of the particles acting as a crystal growth modifier. PVP, SDS, and HPMC behave as growth inhibitors rather than crystal habit modifiers, and barium titanate crystals as small as 26 nm were obtained. D-Fructose appeared to increase the activation energy for barium titanate nucleation when the additive concentration increases. The present study gives new insights into how additives control barium titanate particle growth in aqueous media.

Introduction

Barium titanate ($BaTiO_3$) as a semiconductor exhibits a positive temperature coefficient of resistivity (PTCR) in the polycrystalline form and because of this is used as a thermistor.[1] Barium titanate also exhibits ferroelectric properties and finds wide applications in multilayered ceramic capacitors (MLCCs) and embedded decoupling capacitors (EDC).[1] $BaTiO_3$ is an excellent photorefractive material as well, which justifies its wide application in dynamic holography.[2]

As the miniaturization of electronic devices continues to demand small volumes, the size control of powder precursors is critical. Equiaxed barium titanate nanoparticles have been studied,[3,4] and it was found that decreasing the physical dimension results in the reduction of the spontaneous polarization[5,6] and, consequently, in a change of the functional properties. These observations have stimulated an exponential growth on research aiming to understand the effect of scaling on the ferroelectric properties. Recently, some theoretical studies predicted an enhancement of ferroelectricity in anisotropic "cylindrical" shaped particles[7] and a new kind of ferroelectric order for ferroelectric nanoparticles with one-dimension (1D) structure as nanotubes, nanowires, nanorods, nanobelts, nanofibres.[8]

Morphology control and fabrication of ferroelectric nanoparticles with different shapes are then important. However, the control of the morphology of complex ferroelectric oxides, such as $BaTiO_3$, is not a trivial task and many efforts have been carried out to find efficient and low cost methods capable of producing particles with different shapes and sizes. Indeed, the crystal habit dictates that under equilibrium conditions crystal growth with isotropic morphology will take place for ABO_3 perovskite crystals and round or cubic shaped particles will be easily grown.[9] The growth of anisotropic perovskite particles will not take place spontaneously.

In general, the synthesis approaches for morphological control of nanoparticles can be divided in two main categories. The first one includes template-assisted methods when, either by physical interaction or by chemical reaction the final morphology of the product can be dictated by the size and shape of a template. The second category includes the procedures in which the modification of the crystal growth may occur if the growth on some of the crystal faces will be restricted. This may be achieved by reducing the supply of material to a particular crystal face or by modifying the specific surface energy, that is, in the presence of some additives, named crystal habit modifiers[9] and classified as additive-assisted syntheses.

For the case of ferroelectrics, the most reported approaches for the growth of anisotropic particles are the template-assisted ones. Cylindrical shaped nanoferroelectrics, such as nanorods and nanotubes of $PbZr_xTi_{1-x}O_3$,[10] $BaTiO_3$,[11] and $Sr_xBa_{1-x}TiO_3$,[12] have been grown by physical template procedures. The main drawbacks are the final dimensions because they are confined to the dimensions of the template. Chemical templated methods are based on using precursors with the desired sizes and shapes, which act simultaneously as templates. In principle, small size anisotropic crystalline ferroelectrics can be obtained at low temperatures. However, due to the double role of the templates, as a platform for the growth and chemical precursor, under certain temperature, pressure, and time conditions, the template may lose its anisotropic shape which limits the growth of 1D entities. In the hydrothermal synthesis of $BaTiO_3$ ($T < 200$ °C), starting from layered titanate nanotubes (TiNTs) a phase boundary topotactic reaction on the template tubes surface occurs while at higher temperatures and longer times dissolution−precipitation mechanisms became predominant over the topotactic reaction and tetragonal round shaped and "seaweed" type dendritic particles of $BaTiO_3$ were formed.[13,14] The synthesis of perovskite oxides nanoparticles, with cylindrical shapes, using hydrothermal and related methods is far from being trivial.

Regarding the second category, there are reported examples of additives capable of changing the crystal growth kinetics and so to control the morphology of nanoferroelectric particles. It was experimentally claimed that some polymers could be preferentially adsorbed on specific crystallographic planes and control the crystal growth kinetics.[15,16] Poly(acrylic) acid

*Corresponding author. E-mail: paula.vilarinho@ua.pt; tel: 351 234 370354/259; fax: 351 234 370204.

 Published on Web 08/17/2010

(PAA) and polyethylene-oxide-block-poly(methacrylic) acid adsorb on {100} and {110} crystallographic planes of $BaTiO_3$ and reduce their surface energy.[17] The $BaTiO_3$ particles formed in the presence of these polymeric species were rounder than those formed without any polymeric additives demonstrating the crystal habit modifier role of these polymers.[15] PAA was also used to promote the growth orientation of lead zirconium titanate (PZT) crystals in combination with poly(vinyl alcohol) (PVA).[16] When the synthesis was assisted by PVA that was adsorbed onto (001) crystalline planes of PZT minimizing the surface energy by hydrogen bonding, PZT nanorods were formed. When PAA is added to the system, the surface energy reduction is further enhanced due to the adsorption of PAA through carboxy group bonds, and nanowires of PZT were obtained when both PAA and PVA were used.[16]

Another category of additives, which may influence the growth kinetics and so control the final morphology includes the surfactants. In general, surfactants can influence the growth in two ways: (i) by creating direct micelles (oil in water) the surfactant acts as a growth inhibitor,[18] and (ii) as a capping molecule, they can adsorb on specific crystallographic faces, affecting the growth kinetics, and modifying the crystal shape.[19] Linear alkylbenzene sulfonate (LAS) anionic surfactant was found to act as crystal inhibitor of $BaTiO_3$ nanoparticles.[18] LAS was responsible for the reduction of the particle size of barium titanate powders due to the micelle formation. More recently, surfactant as laurylamine has been found to act as a crystal habit modifier of $BaTiO_3$ by adsorbing on some special crystalline surfaces of the nanoparticles and modifying their growth direction.[19] By an oriented attachment mechanism,[20] well-isolated single-crystalline cubic perovskite $BaTiO_3$ nanorods with diameters ranging from 20 to 80 nm were formed.[19]

Carbohydrates can also affect the crystal growth kinetics and act as crystal modifiers. For example, the polysaccharide hydroxypropylmethylcellulose (HPMC) was found to affect the morphology of polycrystalline copper oxalate particles inducing the precipitation of particles with cubelike to rodlike shapes.[21] HPMC under certain concentrations tends to adsorb specifically in one of the faces of copper oxalate dictating anisotropic crystal growth. The role of crystal modifier of HPMC has been verified in the case of the crystal growth of copper oxalate[22] and $CaCO_3$[23] when the HPMC selectively interacts with the hydrophobic faces of the crystal restricting the crystal growth in one direction. Moreover, the water solution of HPMC is known to present inverse solubility and gelation; this means that HPMC becomes less soluble in water when the temperature increases and eventually becomes a hydrogel with a three-dimensional network.[24]

The effect of additives on the morphological control of $BaTiO_3$ particles has not been addressed systematically. Within this context, in this work different types of additives were tested on the synthesis of $BaTiO_3$ and the structural changes of the nanoparticles assessed and related with the nature of the additive. Poly(acrylic acid) (PAA) and poly(vinylpyrrolidone) (PVP) were used as polymers, sodium dodecylsulfate (SDS) as anionic surfactant, and D-fructose and hydroxypropylmethylcellulose (HPMC) as carbohydrates (saccharides).

Experimental Section

Barium hydroxide, $Ba(OH)_2 \cdot 8H_2O$ (Merck, 98% purity), and titanium *n*-butoxide, Ti(*n*-OBu)$_4$ (Aldrich, 97% purity), were used as barium and titanium precursors, respectively. Poly(acrylic acid) (PAA, Aldrich, $M_w = 2000$), poly(vinylpyrrolidone), (PVP, Acros Organics, $M_w = 8000$), D-fructose (Fru, Acros Organics, 99% purity), hydroxypropylmethylcellulose (HPMC 100, Sigma), and sodium dodecylsulfate (SDS, Aldrich, p.a.) were used as additives. The barium titanate synthesis was initiated by dissolving 7.45 g of $Ba(OH)_2 \cdot 8H_2O$ in 50.7 g of ultrapure distilled water. A supersaturated solution of barium hydroxide was obtained at 90 °C. At this temperature, 50 g of the solution was filtrated and the desired amount of additives were added. Additive concentrations used were 0.4 and 5 g/L for [low] and [high] concentration, respectively. The mixture of barium hydroxide and additives was cooled down to room temperature and 5.7 mL of Ti(*n*-OBu)$_4$ was added under vigorous stirring. A rapid formation of a white precipitate of hydrous titanium oxide in alkaline solution was noticed. The reaction mixture was immersed in a water bath at 96 °C and kept at this temperature for 30 min. In the case of a high concentration of PAA and HPMC, syntheses at temperatures as low as 60 and 80 °C, respectively, were performed in order to better define the additives effect.

The obtained powders are indexed with the abbreviations BTPAA, BTPVP, BTFru, BTHPMC, or BTSDS, corresponding to the additive used in each synthesis. The additives concentrations were indexed as [low] and [high], respectively. BTblank corresponds to the same synthesis but without any additive.

X-ray diffraction (XRD) using a Philips X'Pert diffractometer using Cu-Ka radiation and Raman spectroscopy, recorded on a Bruker RFS 100/S FT Raman spectrometer using a 1064 nm excitation of the Nd/YAG laser, were used for the phase identification of the obtained powders. XRD peak broadening (111) was used to determine the size of the primary crystallites using the Scherrer equation (eq 1).

$$d_{XRD} = \frac{K\lambda_X}{\beta_{Xp} \cos\theta} \quad (1)$$

where K is equal to 0.9, λ_X stands for the X-ray wavelength, β_{Xp} is for the line broadening at half the maximum intensity of the diffraction peak, and θ is the Bragg angle. The instrumental broadening was determined using alumina with a large crystal size ($> 1\ \mu$m).

Powder microstructures were analyzed by scanning electron microscopy (SEM), using a Philips XL 30 FEG microscope.

Brunauer–Emmett–Teller (BET) specific surface areas S_{BET} ($m^2 \cdot g^{-1}$) were estimated from N_2 adsorption isotherms (Micromeritics Gemini 2375). The size of the primary particles, d_{BET} (nm), were calculated by assuming spherical monodisperse particles (eq 2), with ρ as the density of the material ($\rho = 6.017\ g \cdot cm^{-3}$).

$$d_{BET} = \frac{6000}{S_{BET}\rho} \quad (2)$$

Before BET measurements, the samples were dried at 200 °C in flowing nitrogen for 1 h.

Thermogravimetric curves were recorded with a Mettler TGA/DSC/TMA analyzer, from room temperature to 800 °C under air at a heating rate of 10 °C/min.

The particle size distribution (PSD) was collected using a laser diffraction method (Malvern Mastersizer S). 0.4 g of material was dispersed in 40 g of a PAA solution (0.1 wt %, pH = 10) using an ultrasonic horn, before being analyzed (refractive index $n = 2.4$). The median size d_{v50} of the distribution is compared to d_{BET}, to get an estimation of the agglomeration of the particles (F_{agg} is the factor of agglomeration):

$$F_{agg} = \frac{d_{v50}}{d_{BET}} \quad (3)$$

Results

Effect of Polymers (PAA and PVP). Figure 1 presents the X-ray diffraction patterns (Figure 1a) and Raman spectra (Figure 1b) of the samples prepared in the presence of polymers and the blank. The patterns can be indexed to cubic $BaTiO_3$ (JCPDF No. 31-0174). The formation of barium titanate is independent of the PAA or PVP concentration, also confirmed by Raman results (Figure 1b). Cubic $BaTiO_3$ has no permitted Raman modes and for tetragonal $BaTiO_3$ with a space group *P*4*mm* eight Raman active modes are expected, $3A_{1\,g} + B_{1\,g} + 4E_g$.[25] Bands around 517, 253,

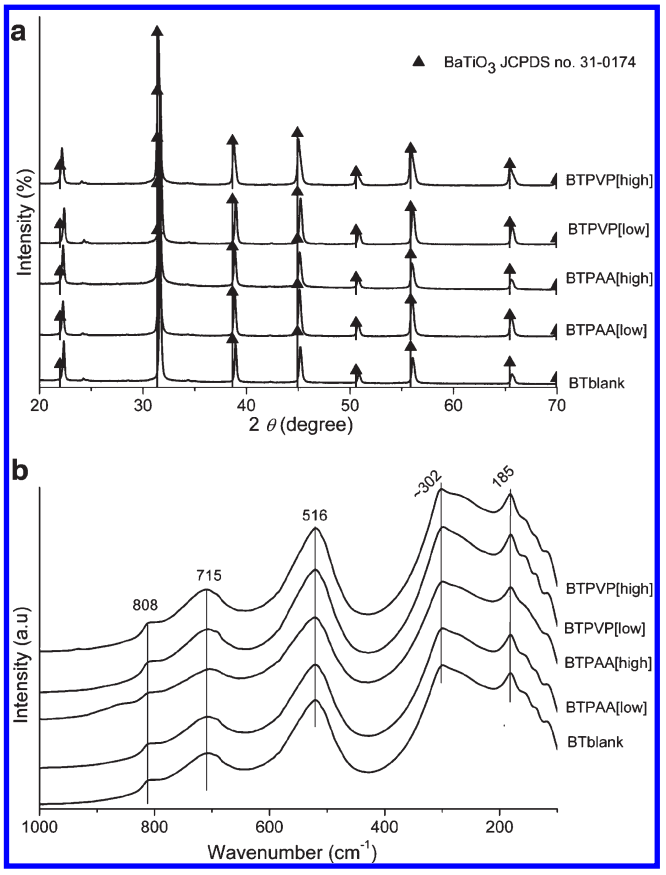

Figure 1. (a) X-ray diffraction patterns and (b) Raman spectra of the samples prepared in the presence of polyelectrolytes - PAA-[low][high] and PVP[low][high] - relative to the blank sample.

Table 1. Specific Surface Areas (S_{BET}), the Equivalent Spherical Particle Diameters (d_{BET}), and the Crystallite Size (d_{XRD}) of the Samples Obtained at 96 °C

sample index	S_{BET} (m^2/g)	d_{BET} (nm)	d_{XRD} (nm)	F_{agg}
BT_{blank}	13.5	74	70	3
$BT_{PAA[low]}$	18.6	54	61	22
$BT_{PAA[high]}$	18.5	54	58	21
$BT_{PVP[low]}$	16.4	61	63	31
$BT_{PVP[high]}$	16.4	61	34	4
$BT_{SDS[low]}$	14.9	67	33	13
$BT_{SDS[high]}$	54.7	18	22	207
$BT_{HPMC[low]}$	19.2	52	65	46
$BT_{HPMC[high]}$	30.5	33	26	69
$BT_{Fru[low]}$	21.0	47	59	39
$BT_{Fru[high]}$	160.0	6	n.a.	n.a.

and 185 cm^{-1} are assigned to the fundamental TO modes (transverse component of the optical mode) of A1 symmetry and the band at 307 cm^{-1} is assigned to the B1 mode, indicating an asymmetry within the TiO_6 octahedra of $BaTiO_3$ at a local scale. The broad band around 715 cm^{-1} is related to the highest frequency longitudinal optical mode (LO) of A1 symmetry. If the sharpness of the peak at 307 cm^{-1} is reduced and it becomes indistinct then the tetragonal phase is not dominant.[26] In the present study, the Raman spectra of the samples synthesized in the presence of polymers present bands at around 185, 300 (small shoulder at ~272) and two sharp peaks at 516 and 715 cm^{-1} (Figure 1b). This result confirms the cubic structure of barium titanate samples synthesized in the polymers presence.

From results shown in Table 1 one can see that at a low polymer concentration S_{BET} is always slightly higher than the one of the blank sample. And in agreement, the crystallite size is lower than the corresponding value of the blank sample. For PVP although no change in S_{BET} with an increase of the additive concentration occurred, the crystallite size decreases from 70 to 34 nm when the concentration of the additive was increased.

Figure 2 presents the SEM micrographs of the blank and the particles prepared in the presence of polymers. Particles synthesized without any additives are small and round shaped with an average diameter of 200 nm (Figure 2a). In the presence of PAA at low and high concentration (Figure 2b,c), barium titanate particles have a morphology similar to the blank sample, the particle size average is ~180 nm, and the degree of agglomeration increases with PAA concentration. In the presence of high PAA content, the particle agglomeration follows a certain alignment as indicated in Figure 2c. The directed aggregation was also observed by TEM (Figure 3). The selected area electron diffraction (SAED) pattern (inset in Figure 3) demonstrates that the aggregation directions are along the [001] direction of the cubic lattice. This is typical for the growth of perovskite crystals where A and B cations have 2^+ and 4^+ valence states, respectively, because the {001} facets are neutral and have the lowest interfacial energy with the surrounding media.[27]

The morphology of the particles obtained in the presence of PVP for low and high concentrations are illustrated in Figure 2, panels d and e, respectively. In both cases, more homogeneous and dispersed particles compared to the blank sample can be noticed which is in agreement with the small agglomeration factor, F_{agg} (Table 1) when the PVP concentration increases.

Figure 4 presents the TGA analysis of the powders obtained with PAA and comparison with the blank sample. The total weight loss includes two important contributions: below ~200 °C, from residual physically adsorbed water, and in the range of ~200−600 °C, from chemically bound hydroxyl groups and decomposition of organic species.[28] The weight losses calculated from the TGA curves for the additive assisted synthesized samples are presented in Table 2. At low concentration of all additives, the weight loss is similar to the blank sample. In the temperature range of 200 to 600 °C, the increase in additive concentration results in a higher weight loss (×2), indicating the polymer adsorption, except for PVP.

Effect of Surfactants. Figure 5 presents the X-ray diffraction patterns (Figure 5a) and Raman spectra (Figure 5b) of the samples prepared from SDS at low and high concentration compared to the blank one. The patterns of these samples are also indexed to a cubic $BaTiO_3$ as in the case of polyelectrolytes. A shift of the X-ray peaks to low angles was observed when SDS was used in low concentration. High concentrations of SDS resulted in a contamination with $BaCO_3$ (Figure 5a). These results are in agreement with the Raman spectra (Figure 5b) where no sharp band is noticed at 307 cm^{-1}, meaning that the barium titanate phase is predominately cubic.

The size of particles synthesized with a low SDS concentration is 50% lower than the blank sample being as small as 33 nm (Table 1). At high SDS concentration, a substantial increase of the specific surface area and an accentuated decrease of the crystallite size is noticed. Round shaped barium titanate with ~150 nm average particle size are obtained in the presence of SDS at low and high concentration (Figure 6a,b). It can be noticed that the degree of agglomeration is higher when SDS is used (Figure 2a), also indicated by the high value of the agglomeration factor, F_{agg} (Table 1).

Effect of Carbohydrates. Figure 7 presents the X-ray diffraction patterns (Figure 7a) and Raman spectra (Figure 7b) of the

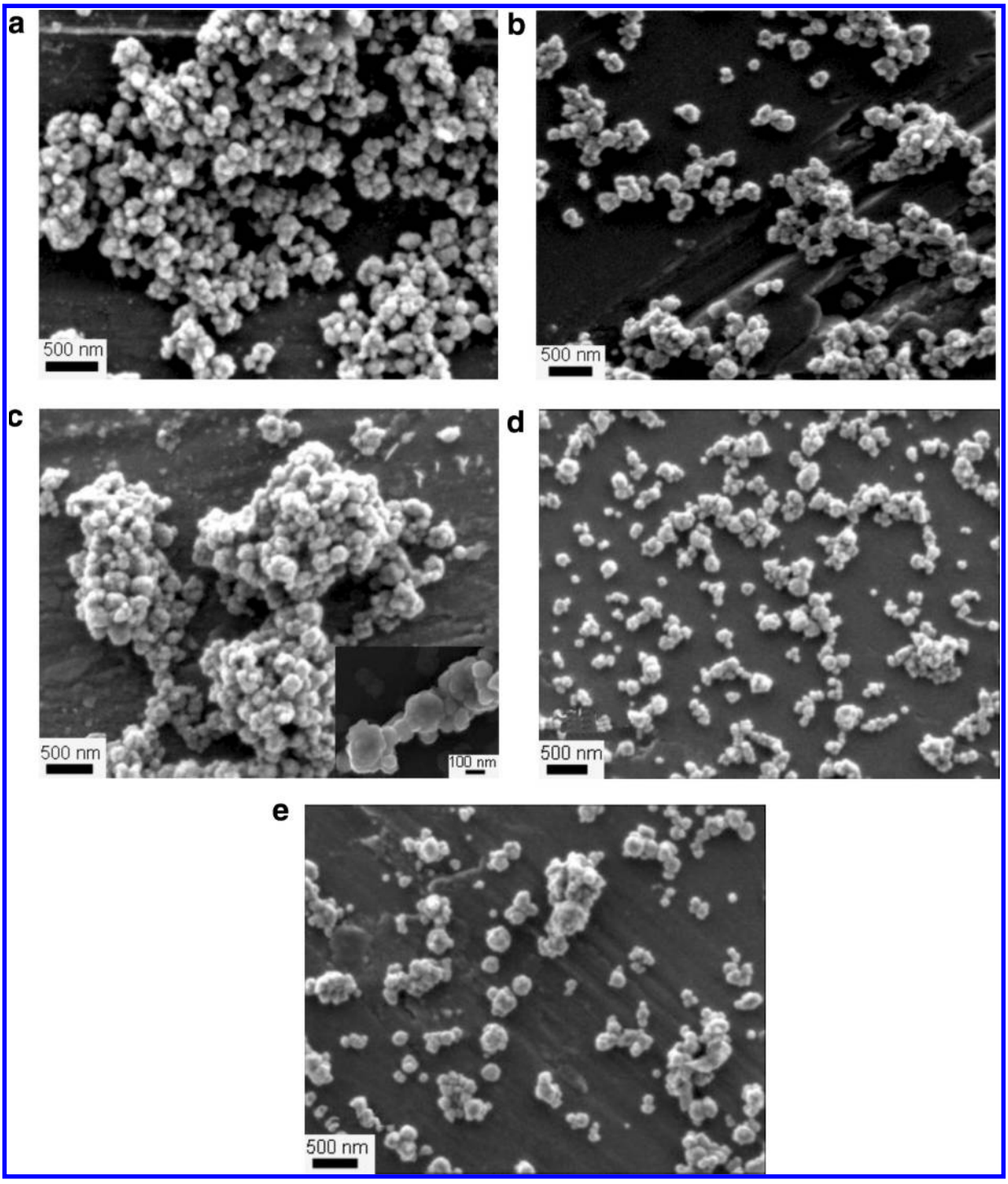

Figure 2. SEM micrographs of (a) blank sample and samples with (b) PAA[low], (c) PAA[high], (d) with PVP[low], and (e) PVP[high].

samples prepared from HPMC and D-fructose at low and high concentrations.

When HPMC is added, cubic barium titanate is formed independent of the additive concentration (Figure 7a), again confirmed by the Raman data (Figure 7b). At high concentration of HPMC, a significant shift of the diffraction peaks to low 2θ angles (Figure 7a) occurs and at the same time barium carbonate is detected. Interestingly, when a high HPMC concentration is used, a substantial increase of the specific surface area and a marked decrease of the crystallite size is observed (Table 1).

In the case of D-fructose, cubic barium titanate is only formed for low additive concentrations (Figure 7a,b). For high concentrations, an amorphous phase together with barium carbonate is identified (see inset of Figure 7a).

Figure 8 presents the SEM micrographs of the samples obtained in the presence of HPMC at low (Figure 8a) and high concentrations (Figure 8b). For the case of low HPMC content, equiaxed particles are observed as in the blank sample (Figure 2a). At high additive amounts, the particles morphology is rather different; it includes small agglomerated particles with rough surface, dendritic particles with a smooth surface and particles with parallelepiped shape (Figure 8b). SEM X-ray mapping confirmed that Ti and Ba are homogeneously distributed in all of the observed morphologies (see inset of Figure 8b).

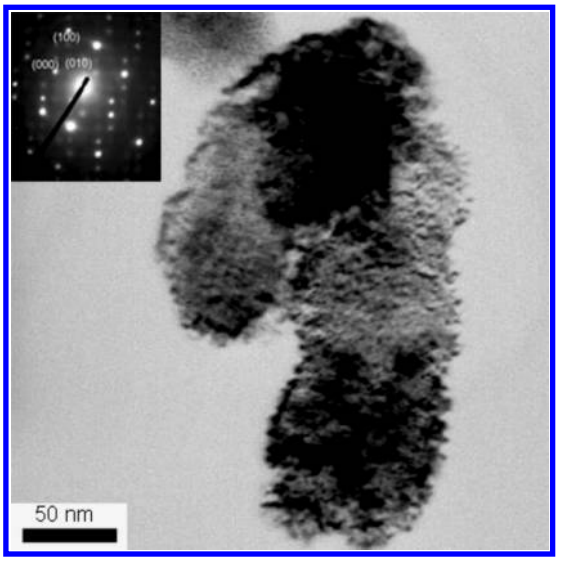

Figure 3. TEM micrograph of the sample prepared in the presence of PAA at high concentration; the inset presents the SAED of this sample.

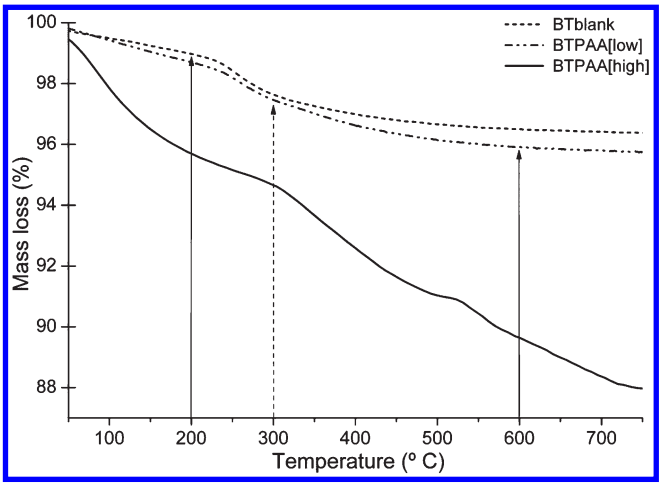

Figure 4. TGA curves of the samples prepared in the presence of PAA at [low] and [high] concentrations relative to the blank sample.

Table 2. Weight Loss of the Samples Calculated from TGA Curves

	mass loss (%)		
sample	< 200 °C	200−600 °C	600−800 °C
BT_{blank}	0.3	2.4	0.2
$BT_{PAA[low]}$	0.3	2.8	0.3
$BT_{PAA[high]}$	0.9	5.8	1.8
$BT_{PVP[low]}$	0.3	2.5	0.3
$BT_{PVP[high]}$	0.3	2.6	0.2
$BT_{SDS[low]}$	0.4	2.5	0.2
$BT_{SDS[high]}$	0.8	4.8	0.4
$BT_{HPMC[low]}$	0.3	2.8	0.2
$BT_{HPMC[high]}$	0.5	6.3	0.2
$BT_{Fru[low]}$	0.6	2.3	0.3
$BT_{Fru[high]}$	2.1	5.9	1.0

For the samples synthesized in the presence of a low concentration of D-fructose, equiaxed barium titanate particles are formed similar to all the previous ones (Figure 9a). However, at high concentrations of D-fructose, large agglomerates of equiaxed particles, which seem to be organized into an ordered porous structure, were formed (Figure 9b). The porous nature of these particles is in agreement with the very high specific surface area (Table 1) and the highest weight loss below 200 °C (Table 2) obtained for high concentrations of D-fructose.

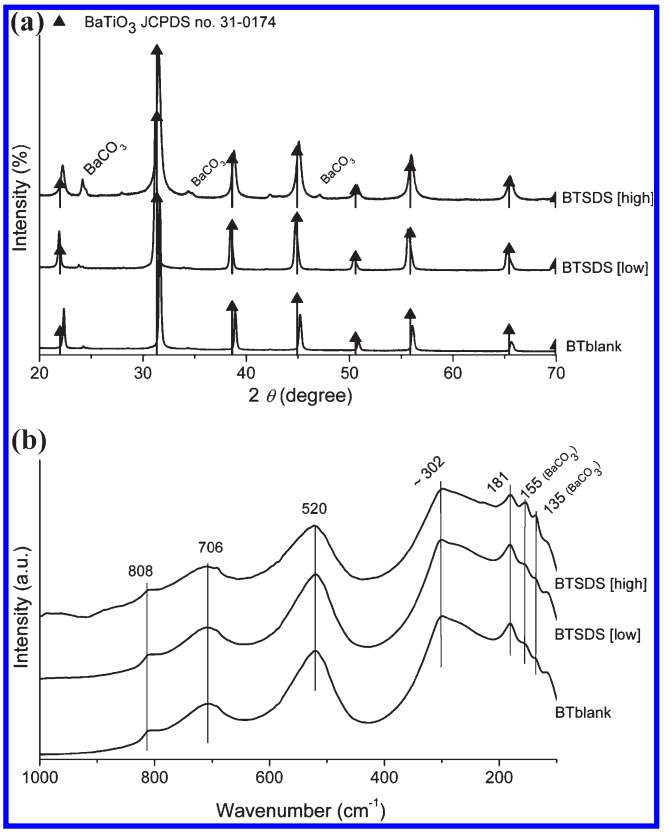

Figure 5. (a) X-ray diffraction patterns and (b) Raman spectra of the samples prepared in the presence of an anionic surfactant SDS[low] and [high] concentrations relative to the blank sample.

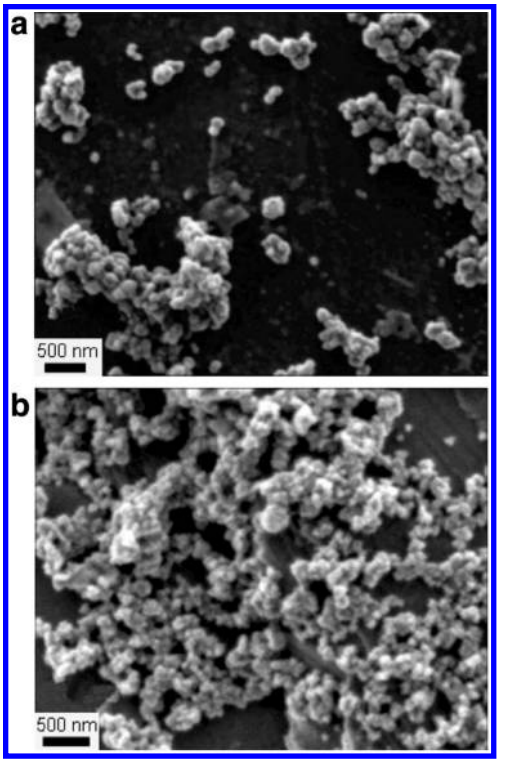

Figure 6. SEM micrographs of the samples prepared in the presence of (a) SDS[low] and (b) SDS[high].

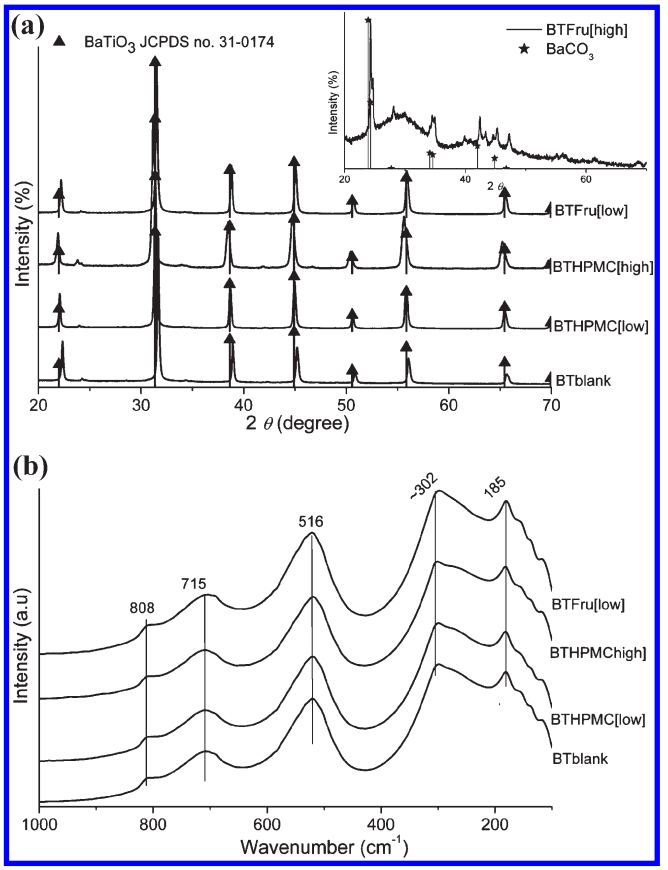

Figure 7. (a) X-ray diffraction patterns and (b) Raman spectra of the samples prepared in the presence of carbohydrates HPMC[low] and [high] concentration and D-fructose[low] (D-fructose[high] in the inset) relative to the blank sample.

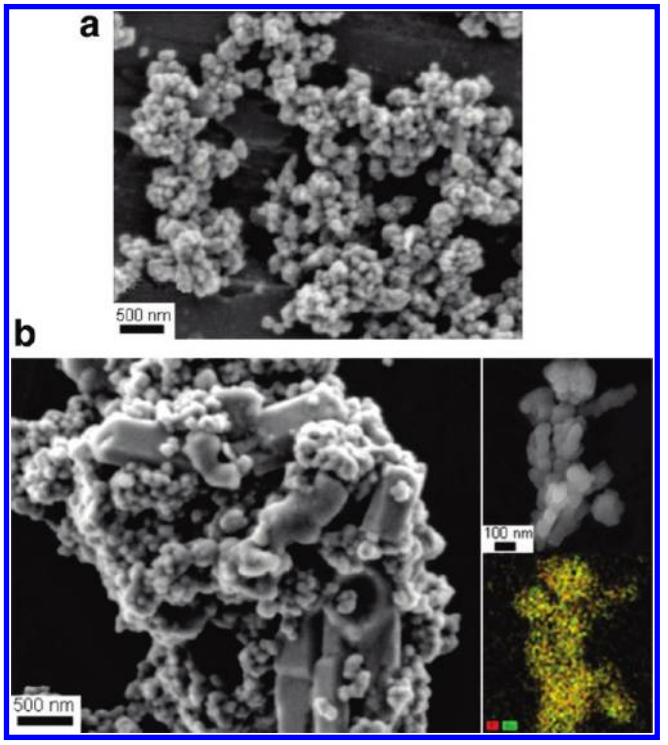

Figure 8. SEM micrographs of the samples prepared in the presence of (a) HPMC[low], (b) HPMC[high]; the inset presents the SEM X-ray mapping of the sample with HPMC[high].

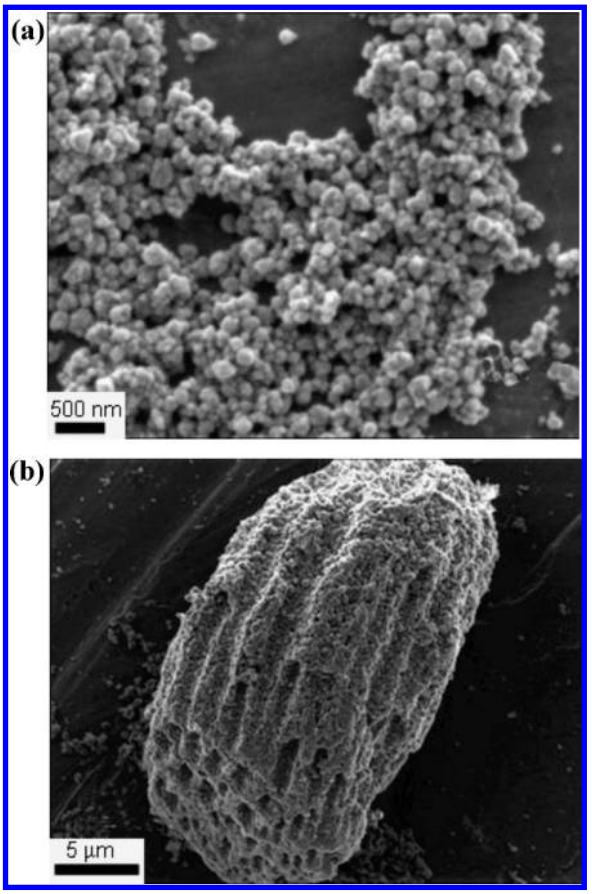

Figure 9. SEM micrographs of the samples prepared in the presence of (a) Fru[low] and (b) Fru[high].

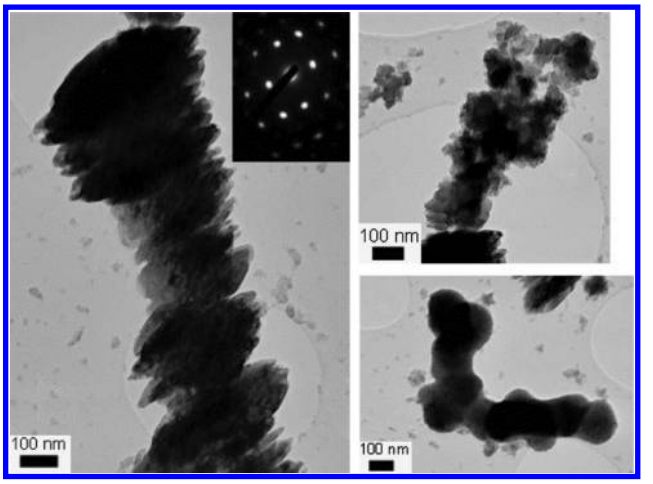

Figure 10. TEM micrographs of the samples prepared at 80 °C in the presence of PAA at high concentration.

Considering that the crystallization process at 96 °C is quite fast (only 30 min are sufficient for the formation of $BaTiO_3$) experiments at lower temperatures were carried out. Little effect was seen except for PAA assisted BT synthesis. Figure 10 presents the TEM images of the obtained sample, mainly represented by amorphous round shaped particles with small sizes illustrated in the left insets. However, few particles with crystalline features, shown in the right side of Figure 10b, are also present in which directed aggregation along the [100] direction of cubic $BaTiO_3$ (see SAED inset) is

Table 3. Summary of the Main Results

	[additive]	crystallographic phase	microstructure	weight loss compared with blank	particle size compared with blank	d_{XRD} compared with blank
PAA	low	$BaTiO_3$	isotropic aggregates of round shape	=	slightly ↑	slightly ↓
	high	$BaTiO_3$	directed aggregation of round shape	2×	slightly ↑	slightly ↓
PVP	low	$BaTiO_3$	dispersed round shape	=	slightly ↑	slightly ↓
	high	$BaTiO_3$	dispersed round shape	=	slightly ↑	1/2
SDS	low	$BaTiO_3$	round shape	=	slightly ↑	1/2
	high	$BaTiO_3$+ $BaCO_3$	round shape	2×	↑	1/3
HPMC	low	$BaTiO_3$	round shape	=	slightly ↑	slightly ↓
	high	$BaTiO_3$+ $BaCO_3$	round shape	2×	↑	1/3
Fru	low	$BaTiO_3$	round shape	=	slightly ↑	slightly ↓
	high	$BaCO_3$ amorphous material	porous cocoon shape	2×	9×	n.a.

visible, similar to the sample prepared at 96 °C (Figures 2c and 3). These results suggest that PAA definitively promotes oriented attachment of the $BaTiO_3$ particles.

Discussion

The results presented above and summarized in Table 3 indicate that crystalline barium titanate can be synthesized in the presence of PAA, PVP, SDS, and HPMC at both low and high concentrations, the only exception being the sample prepared with high concentrations of D-fructose in which $BaTiO_3$ is not formed. However, there are noticeable differences in the morphology of $BaTiO_3$ particles: PAA promotes oriented aggregation of $BaTiO_3$ particles; increasing PVP and HPMC concentration decreases the crystallite size, and the smallest crystallite size is obtained when SDS was used.

Kinetic growth factors can be drastically changed by the presence of additives, which can preferentially adsorb on a specific crystal face. The strength of the adsorption processes influences the change of the crystal habit. From the values of the total weight loss (Table 2), one can observe that all the additives are adsorbed to the barium titanate particles surface at high concentration. However, is the adsorption of the additives effectively changing the growth kinetics in order to change the crystal habit?

Increasing the PAA concentration promotes the direct aggregation of $BaTiO_3$ particles (Figures 2c, 3, and 10). There are two main ways of PAA adsorption at high pH; one is through hydrogen bonding and the second one is by specific bonding of the polymer to charged sites at the surface.[15] The PAA is fully ionized at the working pH (> 12) and so free COO^- groups are present along the polymer chain. Taking into account that at pH >10 barium titanate particles have negative surface charges,[29] the most probable adsorption mechanism of PAA on the particles surface is by specific bonding created by Ba bridges.[30] However, this situation is favored by the formation of monodentate Ba-PAA complex (Ba^+-COO). If Ba^{2+} ions form strongly bounded bidentate species, no positive charge remains to bind the polymer with the barium titanate surface sites and then the polymer is rather trapped during the precipitation than adsorbed to the particle surface. The porous features of $BaTiO_3$ particles prepared with PAA (Figures 3 and 10) and the similar values of S_{BET} independent of the additive concentration are an indication of the trapping of at least some PAA during $BaTiO_3$ precipitation. Therefore, in the present conditions, PAA influences $BaTiO_3$ nucleation by modifying the quantity of the Ba^{2+} in solution. The direct aggregation observed when PAA concentration increases (Figures 2c, 3, and 10) indicates that this additive also influences the growth of $BaTiO_3$. These results suggest that the growth process is controlled by an aggregation mechanism called oriented attachment.[31] A similar mechanism has been reported for the growth of anisotropic $KNbO_3$ nanorods[32] and anatase nanoparticles.[31] The oriented attachment takes place when two adjacent particles come into the same crystallographic orientation, with high-energy faces, fuse and eliminate these faces, and the result is an aggregate with directed orientation.[33] It is then suggested that in the present study PAA could preferentially adsorb on high energy $BaTiO_3$ crystallographic faces, decreasing the growth rate of these faces and inducing the oriented attachment of $BaTiO_3$ particles. It can be therefore stated that PAA limits the growth kinetics of $BaTiO_3$ by decreasing the surface energy and so decreasing the growth rates of specific crystallographic faces. So PAA both adsorbs onto high energy surfaces and is trapped during the precipitation.

PVP is a water-soluble polymer made from the monomer N-vinyl pyrrolidone with a basic character.[34] PVP is a strong Lewis base and may strongly interact with other molecules by the formation of hydrogen bonds and act as a proton acceptor. Because of these properties, PVP can be bonded to surface ions and can form a protection layer, which impedes further aggregation, acting as both growth inhibitor and dispersant.[35] This situation was observed in the case of Ag particles growth when smaller particles were formed due to the protection layer formed by coordinative bond between Ag^+ and nitrogen atoms of PVP.[35] As shown in Figure 1a, monophasic $BaTiO_3$ is formed for both PVP concentrations and the particles morphology is not changed in the presence of PVP. Round shaped particles with diameters between 80 and 100 nm similar to the blank samples have been obtained. Thermogravimetric analysis (Table 2) suggests that no effective adsorption of this polymer on the surface of barium titanate particles takes place even at a high concentration. On the other hand, compared to the blank sample more disperse and homogeneous particles are formed (Figure 2d,e); one cannot have steric repulsion unless the PVP adsorbs. In addition, the increased stability of $BaTiO_3$ suspension could be related to the high viscosity of PVP aqueous solutions,[36] which reduces the mobility of the stable nuclei and consequently the agglomeration. The reduction of the crystallite size (Table 1) from 70 nm (for the blank) to 63 nm (for low PVP concentration) and to 34 nm (for high PVP concentration) also indicates that PVP is influencing the growth of $BaTiO_3$ but is not acting as a crystal habit modifier.

SDS is an anionic surfactant with critical micelle concentration of 0.252 g/100 cm^3 at 30 °C.[37] It is known that the critical micelle concentration increases with the temperature and decreases with the increase of the ionic strength. In alkaline medium, the ionic strength is higher as the pH increases. Under the present experimental conditions (pH > 12 and SDS concentration more than 0.4 g/L), SDS is forming micelles. The X-ray patterns (Figure 5a) show that barium titanate phase was obtained for both SDS concentrations; however, a significant

amount of barium carbonate is formed at high SDS content. This result, supported by the high S_{BET} (porous structure due to unreacted titanium hydroxide gel[38]) observed when high concentrations of surfactant (Table 1) were used, indicates that SDS is avoiding or delaying the reaction between barium and titanium species, and so $BaTiO_3$ nucleation. Surfactants can influence the growth in two ways: as a growth inhibitor when creating micelles[18] and/or as a crystal shape modifier when acting as a capping molecule.[19] In the present study, SDS acted rather as a growth inhibitor than as a crystal modifier as the crystallite size is drastically reduced when using SDS (Table 1) and no changes in the particle shape have been noticed. However, the colloidal stability was reduced when using SDS and more agglomerated powders were obtained (Figure 6 and Table 1).

HPMC is a polysaccharide chemically derived from cellulose by insertion of hydrophobic moieties such as hydroxypropyl and methyl. Despite the introduction of these hydrophobic groups, HPMC presents a linear polymeric chain with a high hydrophilic character due to the presence of polyhydroxy groups on the molecular chains, which make the polymer water-soluble.[39] The hydrophobic parts of HPMC are important for its surface activity (as in a polysoap) and unique hydration−dehydration characteristics. At low HPMC concentration, barium titanate growth and all the results are quite similar to the ones obtained for the blank sample. On the contrary, with high HPMC concentrations the synthesis of $BaTiO_3$ was strongly modified: high SBET, high weight loss, and important presence of $BaCO_3$. These results indicate that HPMC delays the reaction between barium and titanium species as observed in the case of SDS, perhaps because HPMC is strongly attached on the titanium hydroxide gel surface and thus impedes its dissolution. Moreover, the crystallite size drastically decreases from 70 nm (in the blank) to 26 nm (at high HPMC concentration) (Table 1) and different morphologies were formed (Figure 8b). These results indicate that HPMC preferentially acts as a growth inhibitor than as a crystal growth modifier. HPMC can act as a growth inhibitor as the crystal growth can be regulated and restricted by the three-dimensional network structure of HPMC gel formed when increasing the synthesis temperature and additive concentration.

In this study, the most evident additive effect on $BaTiO_3$ crystallization was observed for D-fructose. This is a water-soluble monosaccharide with a cyclic structure.[39] Low D-fructose concentration did not affect the formation of $BaTiO_3$ (Figure 7). However, when a high concentration of D-fructose was added, no $BaTiO_3$ was formed (see inset of Figure 7a). Moreover, it is possible that the hydroxyl groups of D-fructose interacted with the barium cations and the titanium hydroxide species forming an intermediary porous amorphous phase (Figure 9b) that should be responsible for the high S_{BET} of the Fru[high] sample (Table 1). This porous structure is very hygroscopic, losing a high percentage of water below 200 °C (Table 2). It is evident then that the energy barrier for barium titanate nucleation is increased as the additive concentration increases. Similar behavior has been observed in the case of $CaCO_3$ crystallization in the presence of saccharides as organic crystal modifiers. The nucleation of calcite was strongly dependent on the saccharide concentration.[40] This behavior is probably an expression of Ostwald's step rule which stipulates that the metastable phase nucleation rate can be higher than those of the stable phase due to the local decrease of the supersaturation.[41] However, how saccharides, in general, and fructose, in particular, affect the crystallization acting as crystal modifiers, it is not yet elucidated. It is proposed that in the particular case of $BaTiO_3$ the local decrease of supersaturation can be due to formation of stable Ba-fructose complexes which restrict the reaction with titanium precursor and so the crystallization of $BaTiO_3$.

Conclusions

Poly(acrylic acid), poly(vinyl pyrrolidone), sodium dodecylsulfate, D-fructose, and hydroxypropylmethylcellulose (HPMC) were used as additives to control the growth of $BaTiO_3$ particles in aqueous synthesis. The structural and chemical nature of each additive governed the interaction behavior with the $BaTiO_3$ particles. At low concentrations, the additives did not affect the crystallization of $BaTiO_3$. For high concentration of PAA, the additive is specifically adsorbed on the $BaTiO_3$ crystallographic planes, decreasing the energy of these faces and promoting the oriented attachment of the particles. PVP seems not to adsorb on $BaTiO_3$ surfaces, but it acts as a dispersive agent and as a growth inhibitor when increasing the additive concentration by modifying the solution viscosity. SDS in high concentration forms micelles, and consequently acts as a growth inhibitor due to the limitation of mass transport of barium and titanium species. The inverse solubility of HPMC with the increase in the additive concentration and synthesis temperature is the reason for $BaTiO_3$ growth inhibition. Finally, D-fructose in high content seems to change the energy barrier of $BaTiO_3$ nucleation presenting a threshold concentration for the nucleation.

Although the present study gives useful insights into how additives control barium titanate growth from aqueous solutions, it demonstrates that the morphological control of complex oxides by chemical methods is complex and suggests that in order to control the morphology of $BaTiO_3$ particles by aqueous synthesis a fast and homogeneous nucleation is required. In addition, among the analyzed additives the most promising crystal habit modifiers seem to be PAA.

Acknowledgment. The authors acknowledge FCT, FEDER, European Network of Excellence FAME, under the contract FP6-500159-1 and Cost Action 539. F.M. is thankful to FCT for the fellowship SFRH/BD/23375/2005.

References

(1) Hennings, D.; Klee, M.; Waser, R. *Adv. Mater.* **1991**, *3*, 334.
(2) Kip, D. *Appl. Phys. B-Lasers Opt.* **1998**, *67*, 131.
(3) Begg, B. D.; Vance, E. R.; Nowotny, J. *J. Am. Ceram. Soc.* **1994**, *77*, 3186.
(4) Buscaglia, V.; Buscaglia, M. T.; Viviani, M.; Mitoseriu, L.; Nanni, P.; Trefiletti, V.; Piaggio, P.; Gregora, I.; Ostapchuk, T.; Pokorny, J.; Petzelt, J. *J. Eur. Ceram. Soc.* **2006**, *26*, 2889.
(5) Frey, M. H.; Payne, D. A. *Phys. Rev. B* **1996**, *54*, 3158.
(6) Uchino, K.; Sadanaga, E.; Hirose, T. *J. Am. Ceram. Soc.* **1989**, *72*, 1555.
(7) Morozovska, A. N.; Eliseev, E. A.; Glinchuk, M. D. *Physica B* **2007**, *387*, 358.
(8) Naumov, I. I.; Bellaiche, L.; Fu, H. *Nature* **2004**, *432*, 737.
(9) Dirksen, J. A.; Ring, T. A. *Chem. Eng. Sci.* **1991**, *46*, 2389.
(10) Limmer, S. J.; Cao, G. *Adv. Mater.* **2003**, *15*, 427.
(11) Hernandez, B. A.; Chang, K.-S.; Fisher, R. E.; Dorhout, P. K. *Chem. Mater.* **2002**, *14*, 480.
(12) Morrison, F. D.; Luo, Y.; Szafraniak, I.; Nagarajan, V.; Wehrspohn, R. B.; Steinhart, M.; Wendorff, J. H.; Zakharov, N. D.; Mishina, E. D.; Vorotilov, K. A.; Sigov, A. S.; Nabayashi, S.; Alexe, M.; Ramesh, R.; Scott, J. F. *Rev. Adv. Mater. Sci.* **2003**, *4*, 114.
(13) Maxim, F.; Ferreira, P.; Vilarinho, P. M.; Reaney, I. *Cryst. Growth Des.* **2008**, *8*, 3309.

(14) Maxim, F.; Vilarinho, P. M.; Ferreira, P.; Reaney, I.; Levin, I. *Chem. Mater*. **2010**, submitted.
(15) Bagwell, R. B.; Sindel, J.; Sigmund, W. *J. Mater. Res*. **1999**, *14*, 1844.
(16) Xu, G.; Ren, Z. H.; Du, P. Y.; Weng, W. J.; Shen, G.; Han, G. R. *Adv. Mater*. **2005**, *17*, 907.
(17) Gruverman, A.; Auciello, O.; Tokumoto, H. *Annu. Rev. Mater. Sci*. **1998**, *28*, 101.
(18) Hung, K. M.; Yang, W. D.; Huang, C. C. *J. Eur. Ceram. Soc*. **2003**, *23*, 1901.
(19) Zhang, S. Y.; Jiang, F. S.; Qu, G.; Lin, C. Y. *Mater. Lett*. **2008**, *62*, 2225.
(20) Penn, R. L.; Banfield, J. F. *Science* **1998**, *281*, 969.
(21) Jongen, N.; Hofmann, H.; Bowen, P.; Lemaitre, J. *J. Mater. Sci. Lett*. **2000**, *19*, 1073.
(22) Jongen, N.; Bowen, P.; Lemaitre, J.; Valmalette, J. C.; Hofmann, H. *J. Colloid Interface Sci*. **2000**, *226*, 189.
(23) Zhao, J.; Li, Y. J.; Kuang, Q. L.; Cheng, G. X. *Colloid Polym. Sci*. **2005**, *284*, 175.
(24) Sarkar, N.; Walker, L. C. *Carbohyd. Polym*. **1995**, *27*, 177.
(25) Asiaie, R.; Zhu, W.; Akbar, S. A.; Dutta, P. K. *Chem. Mater*. **1996**, *8*, 226.
(26) Joshi, U. A.; Yoon, S.; Balk, S.; Lee, J. S. *J. Phys. Chem. B* **2006**, *110*, 12249.
(27) Mitchell, R. H. *Perovskite-Modern and Ancient*; Almaz Press Inc.: Ontario, Canada, 2002.
(28) Ciftci, E.; Rahaman, M. N. *J. Mater. Sci*. **2001**, *36*, 4875.
(29) Chen, Z. C.; Ring, T. A.; Lemaitre, J. *J. Am. Ceram. Soc*. **1992**, *75*, 3201.
(30) Pochard, I.; Couchot, P.; Foissy, A. *Colloid Polym. Sci*. **1998**, *276*, 1088.
(31) Penn, R. L.; Banfield, J. F. *Geochim. Cosmochim. Acta* **1999**, *63*, 1549.
(32) Magrez, A.; Vasco, E.; Seo, J. W.; Dieker, C.; Setter, N.; Forro, L. *J. Phys. Chem. B* **2006**, *110*, 58.
(33) Meldrum, F. C.; Colfen, H. *Chem. Rev*. **2008**, *108*, 4332.
(34) Bury, R.; Desmazieres, B.; Treiner, C. *Colloids Surf., A* **1997**, *127*, 113.
(35) Wang, H.; Qiao, X.; Chen, J.; Wang, X.; Ding, S. *Mater. Chem. Phys*. **2005**, *94*, 449.
(36) Kobayashi, Y.; Kosuge, A.; Konno, M. *Appl. Surf. Sci*. **2008**, *255*, 2723.
(37) Sovilj, V. J.; Petrovic, L. B. *Carbohydr. Polym*. **2006**, *64*, 41.
(38) Brinker, C. J.; Scherer, G. W. *Sol-Gel Science*; Academic Press: New York, 1990.
(39) Isbell, H. S. *Carbohydrates in Solution*; American Chemical Society: Washington, DC, 1973.
(40) Dickinson, S. R.; McGrath, K. M. *Cryst. Growth Des*. **2004**, *4*, 1411.
(41) Markov, I. V. *Crystal Growth for Beginners*; World Scientific Publishing Co. Pte. Ltd.: Hackensack, NJ, 1995.